

Protrusions fluctuations direct cell motion

David Caballero^{1,2}, *Raphaël Voituriez*^{3,4}, *Daniel Riveline*^{1,2,*}

¹ Laboratory of Cell Physics, ISIS/IGBMC, Université de Strasbourg and CNRS (UMR 7006), 8 allée Gaspard Monge, 67083 Strasbourg, France

² Development and Stem Cells Program, IGBMC, CNRS (UMR 7104), INSERM (U964), Université de Strasbourg, 1 rue Laurent Fries, BP10142, 67400 Illkirch, France

³ Laboratoire de Physique Théorique de la Matière Condensée, CNRS UMR 7600, Université Pierre et Marie Curie, 4 Place Jussieu, 75005 Paris, France

⁴ Laboratoire Jean Perrin, CNRS FRE 3231, Université Pierre et Marie Curie, 4 Place Jussieu, 75005 Paris, France

*Corresponding author: Daniel Riveline; e-mail: riveline@unistra.fr; Laboratory of Cell Physics, ISIS/IGBMC, Université de Strasbourg and CNRS (UMR 7006), 8 allée Gaspard Monge, 67083 Strasbourg, France. TEL: +33 (0) 3 68 85 51 64; FAX: +33 (0) 3 68 85 52 32.

Abstract

Directional cell migration is a process involved in many physiological phenomena being mainly associated to chemical cues *in vivo*. Recently, *in vitro* cell guiding assays have been realized by means of stiffness/adhesion gradients or micro-patterned adhesive motifs. The cellular mechanisms leading to biased migration remain however widely unknown and often even the direction of motion is unpredictable. In this study, we show the key role of fluctuating protrusions on ratchet-like structures for driving cell migration. We identified the concept of *efficient protrusion* and associated direction index. Our analysis of protrusion statistics enabled the quantitative prediction of cell trajectories in situations where we varied external cues (adhesive patterns) and internal cues (protrusion activity), and strikingly even made possible to sustainably drive cell motion in the direction opposite to that predicted by their imposed polarization. Based on only two measured cellular parameters at short timescales, we developed a theoretical model showing that asymmetry of protrusion activity and their stabilization are sufficient for predicting all measures associated with long-term motion. Altogether this study provides a new framework for explaining cell motion as a persistent random walk.

Introduction

Cell migration is involved in many physiological processes such as tissue development or immune response [1, 2] as well as in some pathological phenomena such as tumor invasion or cancer metastasis [1-4]. Different studies have described this phenomenon mainly as a consequence of chemical cues and growth factors that lead to the regulation of signaling networks [5, 6]. Mechanical cues can also be used to direct cell motion [7-9]. As an example, on surface gradients of adhesive proteins, cells migrate directionally towards regions of larger concentrations. Similarly, on gradients of substrate rigidity cells move towards regions of higher rigidity [7, 8, 10]. However, in general, cells are not moving along

directions that are set by simple rules, thereby preventing quantitative prediction for the motion. Indeed, little is known about how the dynamics of fluctuating protrusions (filopodia and lamellipodia) of the cytoskeleton are involved in guiding cell migration. On homogenous and isotropic 2-D surfaces, cell protrusions show highly dynamic and random fluctuating behaviors essentially because fibronectin is always present: this stabilizes protrusions that are extended in any direction and causes the cell to perform a non-directional random motion. This calls for new concepts in predicting cell motion in general situations.

Fluctuations have been shown to play an essential role in many biological systems, such as in molecular motors motion [11]. This idea was pioneered by Richard Feynman in his ratchet and pawl chapter [12], where he showed that non-directional motion driven by fluctuation is rectified by breaking time and spatial symmetry. Inspired by this framework we aim to understand how the fluctuations of protrusions regulate directional cell motion. In particular, we examined how cells behave in environments where only protrusions activity triggers cell motility without other regulatory mechanisms, such as chemoattractants. For that purpose, we plated cells on a series of adhesive patches that have asymmetric triangular shapes and are separated by non-adherent gaps. This set-up guided asymmetrically the growth and dynamics of cell protrusions towards the neighboring triangles.

Stochasticity could be quantified in this set-up by measuring the frequencies of protrusions extending and adhering. We found that cells extended protrusions more frequently from the wide end of triangular patch compared to its sharp end, whereas protrusions extending from the sharp end were more stable than those from the wide end. As a result, cells directions were possible in either directions; however on average, cells migrated mostly towards the direction defined by the sharp end in both short and long-term experiments of cell moving over days, and yet this is the timescale that is most relevant for development or physiological processes. Furthermore, by regulating the cytoskeleton dynamics by

inhibiting the Rho and Rac pathways, we altered the nature of protrusions fluctuations and modified the motion of cells on the same ratchets. In all cases, we could define and measure frequencies of probing and adhering.

A simple mesoscopic model based on persistent random walk using the biased probabilities of protruding and adhering was developed. The model was able to efficiently predict the long-term ratchet efficiency and the persistence length by means of only two measurable parameters. These results demonstrate that the asymmetry of the frequency and stabilization time of protrusions are key physical parameters that determine the direction of cell motion.

Results

We designed an assay where we plated NIH3T3 fibroblasts (ATCC) on a series of adhesive micropatterned (fluorescent fibronectin, Cytoskeleton, 10 $\mu\text{g ml}^{-1}$) (see Fig.1(a)-(b)) [13-15]; the selected concentration corresponds to near the optimal in the dumbbell motility curve [16] (see Supplementary Figure SF1). The area of each patch, 1590 μm^2 , corresponds to the mean cell area on non-patterned surfaces (see Supplementary Figure SF2). The structures have asymmetric triangular shapes; they are separated by non-adherent gaps of 20.5 μm , corresponding to near the average protrusion lengths d_p (see Supplementary Figure SF2, SF3 and Supplemental Methods). The non-patterned regions were passivated by non-adherent 0.1 mg ml^{-1} PLL-g-PEG (SuSos) forcing cells to extend protrusions to probe the adhesive regions at the nearest neighbor (Fig.1(c) and Supplementary Methods). This feature is in contrast to the situation of cells on uniform 2D surfaces and on micropatterned surfaces of connected adhesive patches [17] that show continuous cycles of protrusions-retractions. This set-up guided asymmetrically the growth and dynamics of cell protrusions towards the neighboring triangles.

To move to the neighboring adhesive patches, cells must extend filopodia that are longer than the gap. This implies that the direction of cell motion may be determined by the asymmetry of protrusions. We therefore observed filopodia with an inverted microscope (Olympus) (40X 0.65 N.A. phase-contrast air objective, 37°C, 1% bovine calf serum (BCS) L-15 medium (Invitrogen)) (see Fig.1(c), Supplementary Movie SM1). We first measured that cells extend protrusions of similar lengths in all directions, and thus probe their surrounding symmetrically on both sides, defined as +/- directions (see Fig.1(c), Supplementary Figure SF3). We assumed that the probability per unit time z of making a productive attachment, which eventually leads to transmission of a force, named *effective protrusion*, is proportional to the intersection of the explored area with the fibronectin pattern. In order to bias the activity of effective protrusions, we designed the ratchet so that the effective adhesion areas differed on both sides ($A_+ \neq A_-$) with the corresponding asymmetry in the activity of effective protrusions $z_+ \neq z_-$ (see Fig.1(c)). We then measured the frequency of probing of filopodia touching the adhesive zones on both sides (ν_+ and ν_-), and found that they were more numerous on the - side (see Fig.1(f)i), but they lasted longer on the + side (dwell time on adhesive patches are denoted τ_+ and τ_-). This suggests that ν_{\pm} and τ_{\pm} are two competing factors that control the activity of effective protrusions.

Assuming that a protrusion can be activated (*ie* generate a force) at a constant rate β when it lies on an adhesive area, the mean number of effective protrusions induced per unit time is given by $z_i = s_i \nu_i \approx \beta \nu_i \tau_i$ and it depends on the side $i=+,-$ (s_i is the probability that a protrusion is activated on side i). We introduce the following parameter ‘*direction index*’ (I_{dir}):

$$I_{dir} = (z_+ - z_-)/(z_+ + z_-) \quad (1)$$

that encodes the asymmetry of efficient protrusion activity and depends only on the parameters ν_i , τ_i , which are accessible experimentally. We show in Supplementary Methods that $I_{dir} = p_+ - p_-$, where p_+ is the probability that an effective protrusion is on side + rather than -. Our central hypothesis is then

that the average direction of an elementary step from one pattern to a neighboring one is dictated by the asymmetry of the number of efficient protrusion, which is directly quantified by I_{dir} .

We found that cells migrated to the $-$ if $I_{dir}<0$, $+$ if $I_{dir}>0$ or any direction if $I_{dir}\approx 0$. The sign of I_{dir} is therefore directly correlated to the direction of motion suggesting that it is a key parameter that determines the direction of cell migration (see Fig.1(g)-1(i)). The ratchet configuration yielded $I_{dir}=0.33$ (see Fig.1(g)), showing that filopodia extensions are more effective in the $+$ direction (see Supplementary Movie SM1), and in agreement with the actual direction of migration. Cells are initially polarized towards the $-$ direction as confirmed by focal contacts distributions and their mean asymmetric areas (Fig.1(h)) (see also Supplementary Figure SF4 [18]). Furthermore, the accessible adhesive area is also larger in the $+$ direction so that eventually efficient protrusions were more numerous at the $+$ edge (see Fig.1(c)). Remarkably, although the morphology of cells initially follows the geometry of triangular motif, these cells reverse their polarity when they migrate to the $+$ direction (see Fig.1(c) and Supplementary Movie SM1).

To further check these ideas, we modified the geometry of the motifs while fixing the gap distance. We first used a pattern where a triangle is surrounded by symmetric rectangles and hence, cells have equal available adhering area ($A_+=A_-$), but with asymmetric protruding distribution ($\nu_->\nu_+$) (Fig.1(d), Fig.1(f)ii, and Supplementary Movie SM2). As expected, the frequency of effective protrusions is larger towards the $-$ direction than towards the $+$ direction, $z_->z_+$, (see Fig.1(f)ii). Indeed, protrusions are stabilized for longer time on the $-$ side than the $+$ side, $\tau_->\tau_+$. This results in a negative value of I_{dir} (-0.57) and predicts that cells migrate towards the $-$ direction, in agreement with experimental observations (see Fig.1(g)-1(i)).

Replacing the triangle by a circular patch (spot) made the pattern $+,-$ symmetric ($A_+=A_-$). In this

situation $\nu_- \approx \nu_+$ and $\tau_- \approx \tau_+$ within the experimental errors, so that $z_+ \approx z_-$ (see Fig.1(f)iii, Fig.1(g) and Supplementary Movie SM3). In this case, $I_{dir} \approx 0$ within the error (Fig.1(g)). As above, I_{dir} correlated with the obtained average motion, here equally probable + and -. I_{dir} sets the direction of motion in all conditions.

We next perturbed the fluctuations of protrusions in the ratchet by using inhibitors of Rac and Rho pathways (hereafter Rac⁻ and Rho⁻) that are known to control the dynamics of the cytoskeleton [19] (see Fig.1(f)iv-v). We used 80 nM C3 Rho-inhibitor (Cytoskeleton) [20] and 100 μ M NSC23766 Rac-inhibitor (Calbiochem) [21]. Accordingly, ν and τ were altered compared to wildtype (WT) cells. Cells probed more often on the + edge in both cases ($\nu < \nu_+$). Similarly, we found $\tau < \tau_+$, which leads to positive I_{dir} values for both cases (0.22 and 0.33 for Rac⁻ and Rho⁻, respectively) (see Fig.1(g)). This predicts that cells migrate towards the + direction, in agreement with experimental observations (Fig.1(i)).

Altogether, the first-step motion of cells confirmed the prediction that I_{dir} dictates the direction of motion. When cells are polarized, they probe their front environment more frequently, but the probability to find a stable attachment site is an important parameter to set the final direction. Overall what matters is the asymmetry for the number of efficient protrusions, which is encoded in z_+ and z_- , and therefore in I_{dir} . In the case of the ratchet pattern, attachments are easier to make on the backward (+) side, and this is enough to reverse the direction of motility.



We next studied the long-term motion for 48h with a low magnification objective (4X 0.25 N.A. phase-contrast). On a line of multiple spots, wildtype cells are able to hop from one patch to the next as shown in Fig.2(a) (see also Supplementary Movie SM4). While sitting on a patch, cells are un-

polarized (Fig.1(b)). As expected, we obtained no bias in this condition (Fig.3(a)). We then used triangular patches; a variety of behaviors were observed, ranging from fluctuating cells (Fig.2(b)i), cells moving directionally either left or right along the ratchet (Fig.2(b)ii) and cells not moving (about 5% of the cells). In some cases, cells which were migrating directionally were also shown to initially fluctuate $+/-$ and then undergo directed motion (Fig.2(b)ii and Supplementary Movie SM5). The average motion is significantly biased in the $+$ direction as demonstrated by the proportion of cells moving $+$ over $-$ ($+/-$). In this case, $+/-$ was 2.5-fold the value obtained for non-polarized cells on circular patches (see Fig.3(a)).

We then examined cell motility using 3 detailed characteristics of the motion (see Fig.3(b)-3(d)): L_p , the persistence length, T_p , the persistence time, and v the velocity during this motion (see Supplemental Methods). Wildtype cells on circular patches showed similar values on both sides for L_p , T_p and v (Fig.3(b)-3(d)). When cells were on triangular patches, they showed an increase in L_p and T_p due to the asymmetry in the fluctuations (Fig.3(b)-3(c)).

If protrusion activities are playing a key role, then perturbing these protrusions should affect the long-term motion of cells. To verify this, we altered the dynamics of the cytoskeleton in cell motion using Rho^- and Rac^- [19, 22]. The cytoskeleton was modified (see Supplementary Figure SF5). Surprisingly, the $+/-$ proportion was not significantly altered (Fig.3(a)). However, the characteristics of trajectories were changed. Rho^- cells were less polarized: cells were less persistent and stopped more often (see Fig.3(b) and Supplementary Figure SF6). However, asymmetry of the ratchet yielded a stronger asymmetry in the efficiency of protrusions (Fig.1(f)v): the probability to go $+$ was therefore larger than the probability to go $-$, yielding eventually a $+/-$ ratio similar to the untreated case. On the contrary, Rac^- enhanced cell polarity and L_p were therefore larger in both directions. The polarity was strong

enough so that the cell, once polarized in the $-$ direction, maintained this direction for longer than in the untreated case, yielding eventually a similar $+/-$ ratio (Fig.3(a)). Other features such as the ratios L_p^R/L_p^L and T_p^R/T_p^L , switching times (Nt^{-1}) and pausing time (T_{pa}) were also supporting this framework (see Fig.3(b)-3(c) and Supplementary Figure SF6).

To understand the large scale properties of cell trajectories, we developed a mesoscopic model that aims at linking the observed persistence and asymmetry in the $+/-$ directions to the fluctuation dynamics of protrusions. The large scale properties of cell trajectories were well captured by a *persistent random walk* model: a cell trajectory is discretized in lattice units ($l.u.$), each elementary step being defined as a transition from one adhesive motif to a neighboring motif, either in the $+$ or $-$ direction (in $l.u.$). One then introduces the conditional transition probabilities π_{ji} where  which are defined as the probability that a cell performs a step in the direction j , knowing that the previous step was performed in direction i (see Fig.4(a)). These quantities (only two of them π_{++} and π_{--} being independent) encode two effects responsible for the direction of migration: the asymmetry of the adhesive motifs, which as shown above, affects the protrusion activity, and the direction of the previous move, which is reminiscent of cell polarity. The observation that  (see Fig.4(a,b)) clearly shows that the memory of the previous move influences the direction of the upcoming move. It is shown in Supplemental Material that the main characteristics of the trajectories can be expressed in terms of π_{ji} . In particular the bias quantified as the ratio of the probabilities Π_+ and Π_- of observing a step in the $+$ or $-$ direction reads

$$\frac{\Pi_+}{\Pi_-} = \frac{1 - \pi_{--}}{1 - \pi_{++}} \quad (2)$$

while the persistence length in the $+/-$ direction is given by

$$L_p^\pm = \frac{1}{1 - (1-q)\pi_{\pm\pm}}, \quad (3)$$

where q accounts for the finite observation time. Figure 4(c) shows that using the measured values of the π_{ji} (see Fig.4(b)), the predictions of both the +/- ratio (quantified by Π_+/Π_-) and the persistence lengths are in very good agreement with observations. Note that only two independent measurements were needed to predict the long term motion. For each condition we measured the transition probabilities $\pi_{\pm\pm}$ and derived the long term parameters L_p and +/-, which matched remarkably well the experimental results without adjustable parameters. Altogether, these results prove that the cell trajectories are well described by the persistent random walk model.

We next aimed at linking the π_{ji} to the protrusion activity, and at making more quantitative our observation that the step direction correlates to the sign of the direction index I_{dir} defined in Eq.(1). We made use of the parameters accessible experimentally: ν_+ (resp. ν_-), and the corresponding probability that a protrusion is stabilized and eventually mediates a force denoted by s_+ (resp. s_-). Following the finding that the direction of motion depends on the direction of the previous move, we stress that the quantities s_i, ν_i, z_i depend also on the direction of the previous move and should be written as s_j, ν_j, z_j (with $i, j = +, -$). We then hypothesized that the direction of motion at each step is dictated by the edge having the largest number of stabilized protrusions. This condition enables an explicit calculation of π_{ji} that reads (see Supplemental Material):

$$\pi_{ji} = e^{-(z_{ji} + z_{-ji})\tau_0} \sum_{k \geq 1} \left(\frac{z_{ji}}{z_{-ji}} \right)^{k/2} I_k(2\tau_0 \sqrt{z_{ji} z_{-ji}}) \quad (4)$$

where I_k denotes the modified Bessel function of the first kind and t_0 the mean duration of a step.

Interestingly, the π_{ji} fully determine the large scale properties of the cell trajectories and depend only on the z_{ji} (and the time scale t_0), which encode the mean number of stabilized protrusions. We finally note that the π_{ji} can be conveniently expressed in terms of I_{dir} and an additional variable ($(z_{ji} + z_{-ji})\tau_0$ for example). The analytical prediction of Eq.(4) then shows that π_{ji} , and therefore the magnitude of the bias, critically depends on the sign of I_{dir} (see Fig.4(d)), confirming the experimental findings (see Fig.1(g)). To further test the model, we made use of the independent measures of I_{dir} and corresponding transition probabilities of Fig.1(g) and 1(i) (which give the π_{ji} values), which allowed for a direct comparison with the prediction of Eq.(4).

Figure 4(d), where a single fitting parameter $(z_{ji} + z_{-ji})\tau_0$ was used, reveals a very good agreement between the theory and experimental values in all tested conditions, and overall validates our approach.

To conclude, our results bring new evidence that fluctuations are key players in directed cell migration. We demonstrate the cellular phenomenon is based on the asymmetry of protrusion activity, quantified by a simple index I_{dir} ; it integrates the probabilities of protruding together with the probabilities of stabilizing protrusions. Finally, we predicted the long-term ratchet efficiency and persistence length using as inputs only two parameters. This simple framework will be useful for future works aiming at predicting cell motilities *in vitro* and *in vivo*.

We acknowledge M. Labouesse (IGBMC, Strasbourg, France), F. Nédélec (EMBL, Heidelberg, Germany), M. Piel (Institut Curie, Paris, France), A. Bershadsky (Weizmann Institute, Rehovot, Israel) and all the members of the Riveline's lab for critical discussions of the manuscript. A. Bornert is acknowledged for technical help. This work was supported by funds from the CNRS, the University of Strasbourg and the ci-FRC of Strasbourg.

References

- [1] G. Faure-Andre *et al.*, *Science* **322**, 1705 (2008).
- [2] R. J. Hawkins, M. Piel, G. Faure-Andre, A. M. Lennon-Dumenil, J. F. Joanny, J. Prost, and R. Voituriez, *Phys. Rev. Lett.* **102**, 058103 (2009).
- [3] C. Carmona-Fontaine, H. Matthews, and R. Mayor, *Cell Adh. Mig.* **2**, 240 (2008).
- [4] L. M. Machesky, *FEBS Lett.* **582**, 2102 (2008).
- [5] P. A. Iglesias and P. N. Devreotes, *Curr. Opin. Cell Biol.* **20**, 35 (2008).
- [6] J. B. Gurdon and P. Y. Bourillot, *Nature* **413**, 797 (2001).
- [7] C.-M. Lo, H.-B. Wang, M. Dembo, and Y.-l. Wang, *Biophys. J.* **79**, 144 (2000).
- [8] J. T. Smith, J. K. Tomfohr, M. C. Wells, T. P. Beebe, T. B. Kepler, and W. M. Reichert, *Langmuir* **20**, 8279 (2004).
- [9] X. Jiang, D. A. Bruzewicz, A. P. Wong, M. Piel, and G. M. Whitesides, *Proc. Nat. Acad. Sci.* **102**, 975 (2005).
- [10] L. Trichet, J. Le Digabel, R. J. Hawkins, S. R. K. Vedula, M. Gupta, C. Ribault, P. Hersen, R. Voituriez, and B. Ladoux, *Proc. Natl. Acad. Sci. U.S.A* (2012).
- [11] K. Kruse and D. Riveline, in *Current Topics in Developmental Biology: Forces and Tension in Development*, edited by E. S. Inc. (Academic Press, 2011), pp. 67.
- [12] R. Feynman, R. Leighton, and M. Sands, *The Feynman Lectures on Physics* Reading, MA, **1**, 41-I, 1963), Reading, MA.
- [13] A. Kumar and G. M. Whitesides, *Appl. Phys. Lett.* **63**, 2002 (1993).
- [14] D. Caballero, J. Samitier, J. Bausells, and A. Errachid, *Small* **5**, 1531 (2009).
- [15] M. Théry, A. Pépin, E. Dressaire, Y. Chen, and M. Bornens, *Cell Motil. Cytoskeleton* **63**, 341 (2006).
- [16] S. P. Palecek, J. C. Loftus, M. H. Ginsberg, D. A. Lauffenburger, and A. F. Horwitz, *Nature* **385**, 537 (1997).
- [17] G. Mahmud, C. J. Campbell, K. J. M. Bishop, Y. A. Komarova, O. Chaga, S. Soh, S. Huda, K. Kandere-Grzybowska, and B. A. Grzybowski, *Nat. Phys.* **5**, 606 (2009).
- [18] G. W. Luxton and G. G. Gundersen, *Curr. Opin. Cell Biol.* **23**, 579 (2011).
- [19] A. Hall, *Science* **279**, 509 (1998).
- [20] H. A. Benink and W. M. Bement, *J. Cell Biol.* **168**, 429 (2005).
- [21] Y. Gao, J. B. Dickerson, F. Guo, J. Zheng, and Y. Zheng, *Proc. Nat. Acad. Sci.* **101**, 7618 (2004).
- [22] M. Machacek *et al.*, *Nature* **461**, 99 (2009).
- [23] N. Xia, C. K. Thodeti, T. P. Hunt, Q. Xu, M. Ho, G. M. Whitesides, R. Westervelt, and D. E. Ingber, *FASEB J.* **22**, 1649 (2008).

Figure captions

Fig.1. First-step cell motion and protrusions activity. **(a,b)** Cells on fibronectin triangular and circular patches, respectively, and stained for actin and paxillin. Scale bar: 40 μm . **(c,d,e)** (*Upper*) Probing activity scheme for all the configurations. A_{-}, A_{+} and z_{-}, z_{+} represent the efficient probing area and protrusions activity, respectively. (*Lower*) Typical first-step cell motion. Scale bars: 50 μm . **(f)** Measurement of ν and τ in the \pm sides. **(g)** The I_{dir} parameter shows a correlation between the obtained values and the migration percentage. (Data set: $n_{ratchet}=4$; $n_{triangle}=4$; $n_{spot}=5$; $n_{C3}=3$; $n_{NSC23766}=4$). **(h)** (*Upper*) Labeling of focal contacts (paxillin) for mean area quantification. Scale bar: 10 μm . (*Lower*) A bias in focal area was obtained for triangle compared to the spot (Data set: $n_{spot}=25$; $n_{triangle}=23$). **(i)** First-step migration assay. (Data set: $(n;N)_{ratchet}=43;5$. $(n;N)_{spot}=46;2$. $(n;N)_{triangle}=39;2$. $(n;N)_{NSC23766}=96;3$. $(n;N)_{C3}=29;4$). Data are presented as mean \pm SEM. * $P<0.001$ (Student's t-test).

Fig.2. Long-term cell motion. **(a)** Time-lapse sequence for 48h of a cell fluctuating on fibronectin circular patches. **(b)** Time-lapse sequence for 30h of a cell *(i)* fluctuating on the ratchet and *(ii)* migrating directionally towards the + end. Scale bars: 100 μm . Time in hh:mm.

FIG. 3. Motion signature of directed cell migration. **(a)** (*Lower*) Ratchet bias after 48h. Three different behaviors were observed: net ratchet to the \pm , $-$ and fluctuating cells with no resulting net motion. (*Upper*) \pm ratio. **(b,c,d)** L_p , T_p and ν representation, respectively. In b, 1 l.u. 'lattice unit' = 126.5 μm . (Data set: $(n;N)_{spot-WT}=90;3$. $(n;N)_{triangle-WT}=121;5$. $(n;N)_{C3}=50;4$. $(n;N)_{NSC23766}=106;3$). Data are presented as mean \pm SEM. * $P<0.001$; ** $P<0.005$; *** $P<0.01$; **** $P<0.05$. (Student's t-test).

FIG. 4. Comparison between model and experiments. **(a)** Schematic for π_{ij} ; the cell moves first along

the dashed lines, and then along the solid lines. **(b)** Measurements for π_{ij} . **(c)** Comparisons between model and experiments for L_p (in *l.u.*) and bias. **(d)** Predictions of π_{++} as a function of I_{dir} given by Eq.(4). The quantity $(z_{ji} + z_{-ji})\tau_0$ is used as fitting parameter. Experimental values are represented for each condition. *Key:* Red, rectangle-triangle-rectangle. Blue, rectangle-spot-rectangle. Black, *NSC23766*- ratchet. Yellow, *C3*- ratchet. Green, *WT*-ratchet.

Figures

Fig. 1

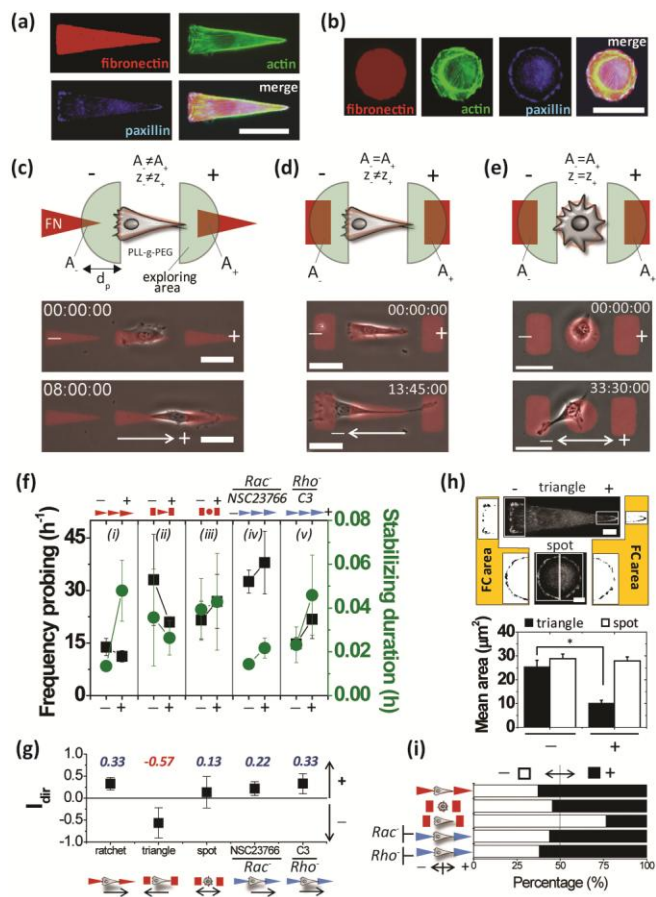


Fig.2

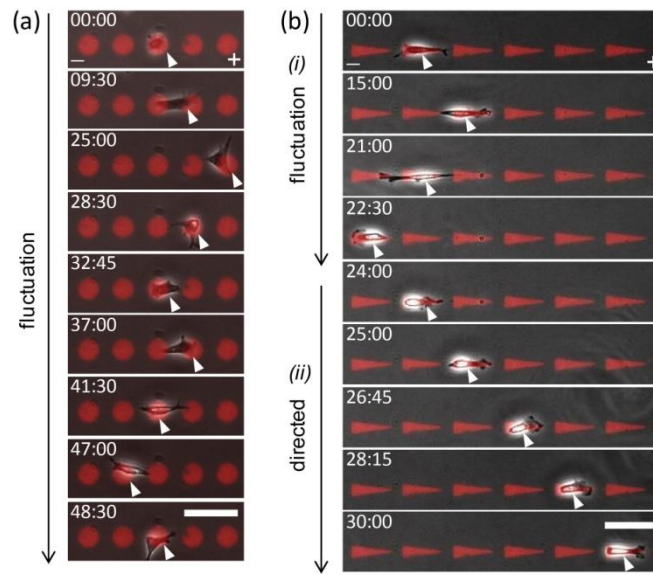


Fig. 3

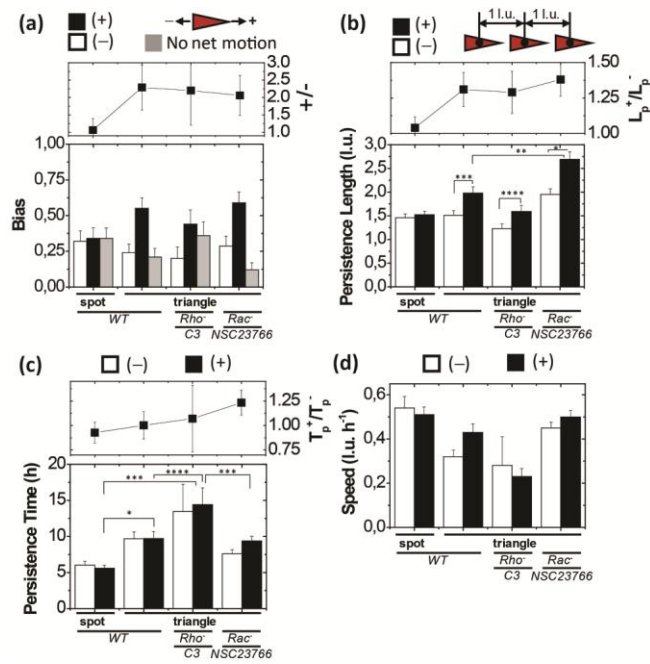
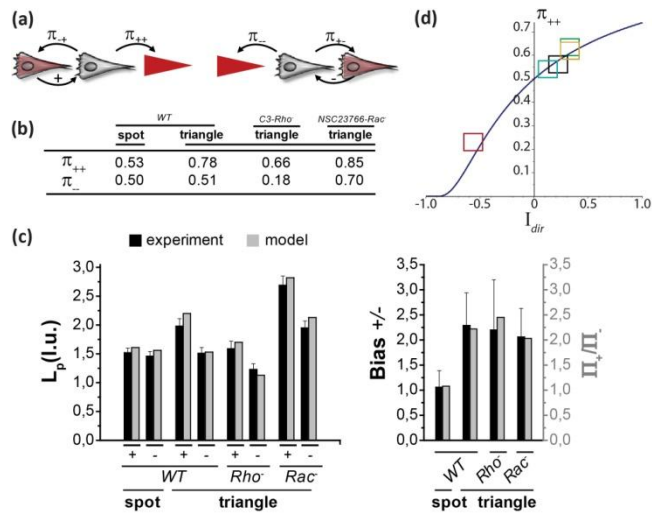


Fig.4



SUPPLEMENTARY MATERIAL

Protrusions fluctuations direct cell motion

David Caballero^{1,2}, *Raphaël Voituriez*^{3,4}, *Daniel Riveline*^{1,2*}

¹ Laboratory of Cell Physics, ISIS/IGBMC, Université de Strasbourg and CNRS (UMR 7006), 8 allée Gaspard Monge, 67083 Strasbourg, France

² Development and Stem Cells Program, IGBMC, CNRS (UMR 7104), INSERM (U964), Université de Strasbourg, 1 rue Laurent Fries, BP10142, 67400 Illkirch, France

³ Laboratoire de Physique Théorique de la Matière Condensée, CNRS UMR 7600, Université Pierre et Marie Curie, 4 Place Jussieu, 75005 Paris, France

⁴ Laboratoire Jean Perrin, CNRS FRE 3231, Université Pierre et Marie Curie, 4 Place Jussieu, 75005 Paris, France

*Corresponding author: Daniel Riveline ; e-mail: riveline@unistra.fr, Laboratory of Cell Physics, ISIS/IGBMC, Université de Strasbourg and CNRS (UMR 7006), 8 allée Gaspard Monge, 67083 Strasbourg, France. TEL: +33 (0) 3 68 85 51 64 ; FAX: +33 (0) 3 68 85 52 32.

1. Supplemental Material and Methods

Fibronectin concentration. The concentration of fibronectin was selected in the following manner: the velocities of cells were measured for various concentrations on homogeneous coated microcontact printed surfaces (see Supplementary Figure SF1 in the Supplementary Material). As reported by Palecek *et al*, a dumbbell shape was recorded with hopping cells in the lower region and crawling cells on the higher density region [10]. In order to acquire long displacements for long-term motion, we selected the higher speeds, while keeping the cells in the crawling regions.

Micropattern fabrication. We used microcontact printing technique for fibronectin micropatterning. The stamps were fabricated using poly(dimethylsiloxane) (PDMS) (Sylgard 184 kit, Dow Corning) and standard soft-lithography techniques. A mould of SU-8 resist (MicroChem Corp.) was fabricated on a silicon wafer (Siltronic) by UV exposure (MJB3 contact mask aligner; SUSS MicroTec) through a photolithography mask (Selba SA) and finally developed by using SU-8 developer (MicroChem Corp.) as described [17]. PDMS stamps were fabricated by mixing the prepolymer and the curing agent in a 10:1 (w/w) ratio as widely described. The stamp was made hydrophilic by using an O₂ plasma cleaner. Afterwards, it was inked for 60 min with a 10 µg ml⁻¹ rhodamine-labelled fibronectin solution (Cytoskeleton Inc) [7], dried and placed in contact with a glass coverslip #1 (Marienfeld GmbH & Co.) for 5 min, which was previously functionalized with 3-(mercaptopropyl)trimethoxysilane (Fluorochem) by vapor phase for 1 h and cured for 4 h at 65°C [9] (see Supplementary Figures SF2 in the Supplementary Material [11]). After releasing the stamp, the sample was cleaned by immersing it successively in PBS (pH 7.4), Milli-Q water and 10 mM HEPES (pH 7.4) solutions. Afterwards, the non-functionalized areas were blocked by immersing the sample in a 0.1 mg ml⁻¹ solution of poly-L-

lysine-g-poly(ethyleneglycol) (PLL-g-PEG) (SurfaceSolutions, SuSoS GmbH) in 10 mM Hepes (pH 7.4) at room temperature for 30 min. Finally, the sample was rinsed with PBS twice and stored in PBS at 4°C before cell deposition for a minimum of 30 minutes.

Experimental system. Mouse NIH3T3 fibroblasts were purchased from the American Type Culture Collection (ATCC). They were grown in high-glucose Dulbecco's modified eagle's medium (DMEM) (InVitrogen) supplemented with 1% Pen Strept antibiotics (InVitrogen) and 10% bovine calf serum (BCS) (Sigma-Aldrich) at 37°C degrees and 5% CO₂. Cells were trypsinised (0.25% Trypsin-EDTA) (InVitrogen), centrifuged and deposited on the microcontact printed substrate at a low density of $1 \cdot 2 \times 10^4$ cells cm⁻² to reduce cell-cell interactions. After 20 min, the medium was removed and changed by fresh medium (DMEM + 10% BCS) to eliminate the non-adhered cells. Finally, the sample was placed in a microscope holder, rinsed with 10% BCS DMEM medium (InVitrogen) twice and 1 ml of 1% BCS L-15 medium (supplemented with 1% Pen Strept antibiotics (InVitrogen)) was added to reduce the deposition of ECM proteins present in the medium around the micropattern.

Optical microscopy. Live cells images were acquired with a CKX41 microscope with a 4X phase contrast objective (Olympus) which allowed to capture simultaneously about 15-25 cells in a single experiment. The microscope was equipped with a cooled charge-coupled device camera (C4742-96-12G04; Hamamatsu) and Wasabi acquisition software (Hamamatsu) equipped with automated scanning stage, 2 shutters (Uniblitz; Vincent Associates), and an Hg lamp (FluoArc, Zeiss) for epifluorescence. For protrusions activity and first-step motion analysis data acquisition frequency was 1 image/30 sec. For long-term experiments data acquisition frequency was 1 image/5 minutes with 1 sec of exposition time. An optical red filter (ThorLabs Inc) and the shutters were used to avoid phototoxicity. A thin

layer of mineral oil (Sigma-Aldrich) was deposited on the sample to avoid medium evaporation. The whole setup was embedded inside a temperature controlled cage at 37°C (IceCube, Life Imaging Services) on an optical isolation table providing a high stability to the set-up which allowed us to observe the motion for 2-4 days without drift.

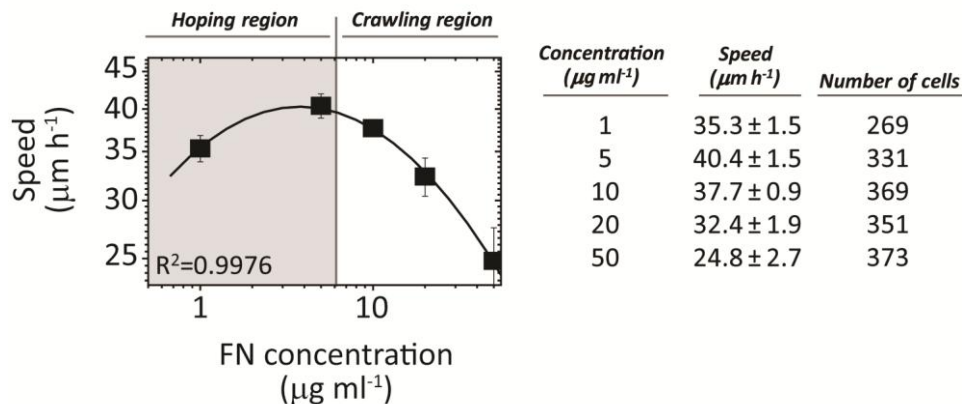
Data analysis. The described biophysical parameters were captured in the following manner. The trajectories of cells were performed by manual tracking by clicking on the centroid of each cell for all the frames (Manual Tracking Plug-in, ImageJ) at 5 minutes interval for 48 hours. Points were connected to generate the migration path which was used to calculate the biophysical parameters. Specifically, we extracted by this method L_p , T_p , v and T_{pa} . Nt^{-1} was recorded as the number of turns that cells had performed during their full motion. Note that N is given by $1/(T_p+T_{pa})$ and v is the ratio of $\langle L_p^i/T_p^i \rangle$, $i=1..n$ cells, and is different from $\langle L_p \rangle / \langle T_p \rangle$ because the distributions are not Gaussian. In order to classify the motions into right (+)/left (-)/no net motion, positions of cells were compared between the starting and the end of the movies. No net motion corresponded to cells going back to the original pattern location, even though cells had been fluctuating right and left during the acquisition. Data were provided as mean \pm SEM. Statistical analysis was carried out by using Student's t -test, and significance was accepted at $P < 0.05$.

Cell fixation and staining. Cells were fixed with 3% paraformaldehyde (Sigma-Aldrich) at 37°C for 17 min or with methanol at -20°C for 10 min for centrosome fixation. Then, 0.5% Triton (Sigma) was added for 3 min to permeabilize cells and the samples were washed twice 5 min with 1X PBS. For staining we used Alexa Fluor 488-phalloidine (Molecular Probes) for actin, rabbit anti-pericentrin (Covance) for the centrosome and DAPI (4,6-diamidino-2-phenylidole, Sigma-Aldrich) for the nucleus.

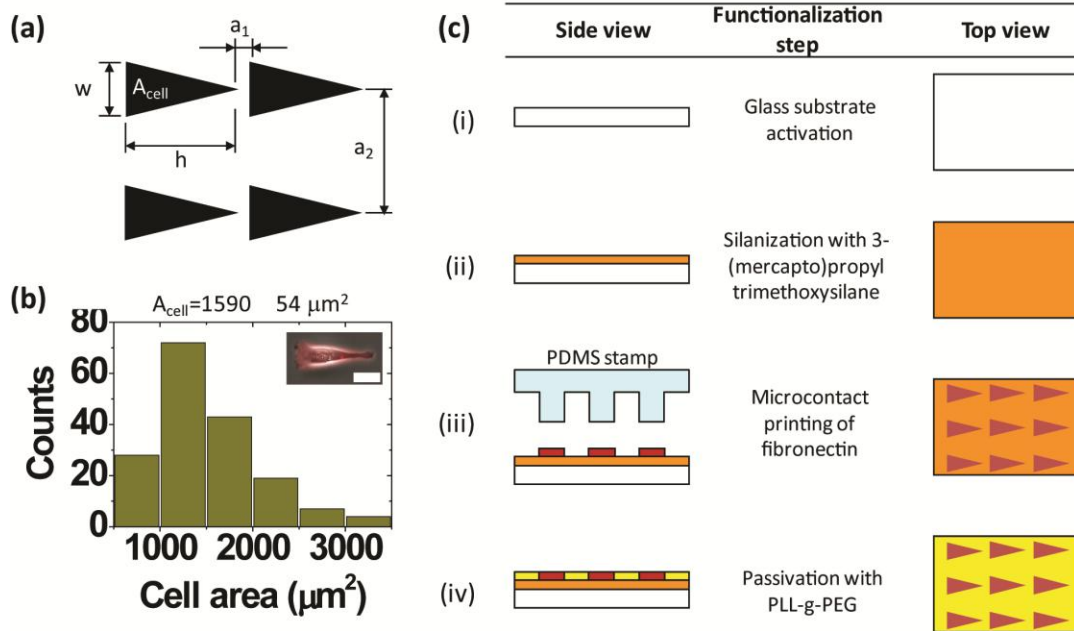
Focal contacts were stained with mouse anti-vinculin or anti-paxillin (Sigma-Aldrich) and microtubules with mouse monoclonal anti-alpha tubulin (Sigma-Aldrich). The following secondary antibodies were used: goat anti-mouse conjugated with Cy3, Alexa 488 goat anti-rabbit (Molecular Probes) and Alexa Fluor 647 goat anti-mouse (Fisher Scientific SAS). All the steps were performed for 45 min at room temperature in PBS. For focal contacts staining on pattern, the steps are performed in PBS with 3% BSA. Then, samples were washed 3 times 5 min with 1X PBS and fixed on 10 μ l drops (50% glycerol, 50% PBS) on a slide.

Stained samples were observed with an inverted fluorescence microscope (Eclipse Ti, Nikon) combined with a Photometrics CoolSNAP HQ² camera. Pre-centered fiber illuminator (C-HGFIE, Nikon) and an X60 oil objective (Nikon) with a numerical aperture of 1.3 were used.

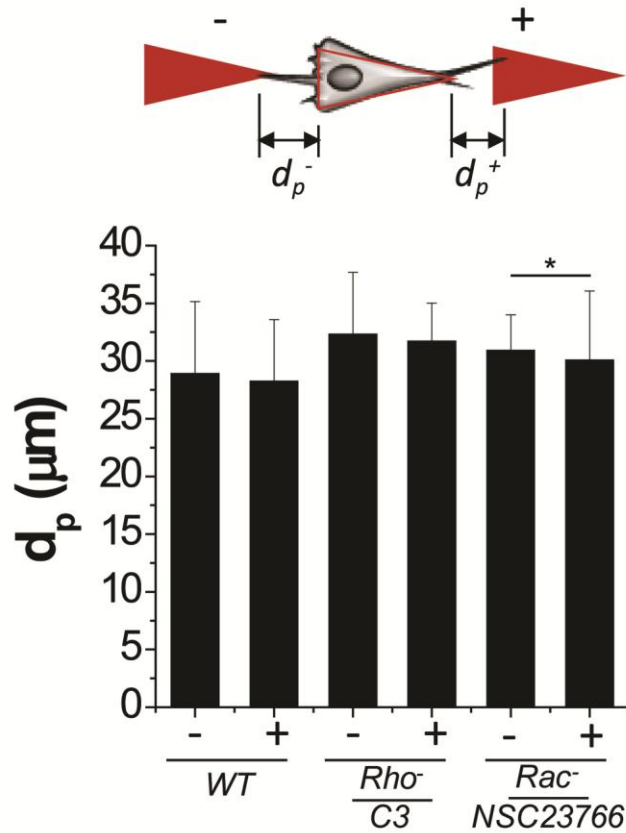
2. Supplemental Figures and Legends.



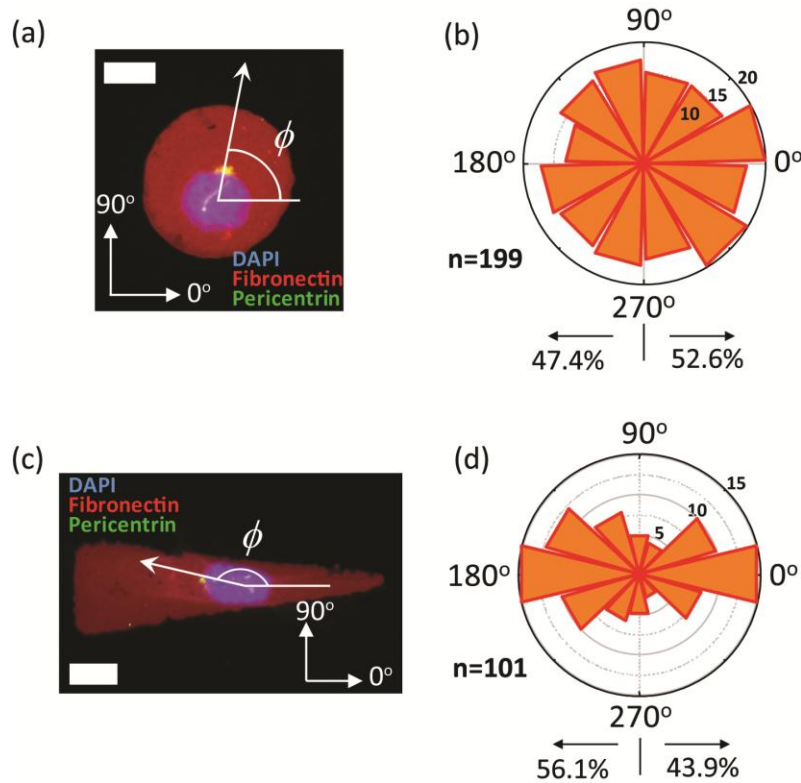
Supplemental Figure SF1. Representation of cell migration speed as a function of fibronectin coating concentration. (Left) Variation of mean cell speed of NIH3T3 cells on homogeneously coated surfaces with fibronectin (FN). The speed is measured by tracking the centroid of each individual cell by determining the initial and final points during which the cell is moving straight. Two different regimes were observed: the first one ranging from $1 \leq [\text{FN}] < 6 \mu\text{g ml}^{-1}$ where cells were hopping, and the second one ranging from $6 \leq [\text{FN}] \leq 50 \mu\text{g ml}^{-1}$ where cells were crawling. The data correspond to N=6 independent experiments for at least 269 cells per condition for a total of n=1693 cells. (Right) Table showing the speed obtained for each fibronectin concentration with the number of cells analyzed per condition. Values are shown as mean \pm SEM.



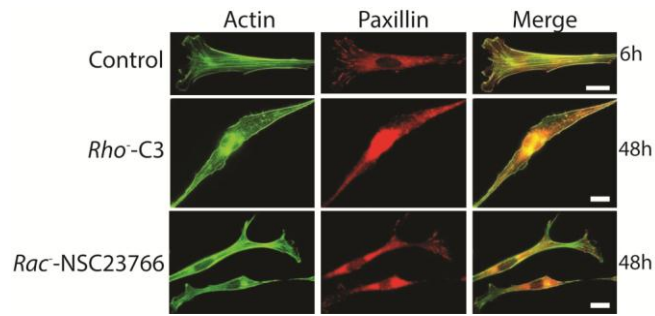
Supplemental Figure SF2. Ratchet design and protocol for the fabrication of the substrates for cell migration study. (a) Micropattern design showing the different used values. $w=30 \mu\text{m}$; $h=106 \mu\text{m}$; $a_1=20.5 \mu\text{m}$; $a_2=200 \mu\text{m}$ and $A=1590 \mu\text{m}^2$. (b) Optimization of micropattern area. Cells were deposited on a microcontact printed glass coverslip with a $10 \mu\text{g ml}^{-1}$ fibronectin concentration and we let them spread. The area of individuals cells ($n=176$ cells) was measured and the averaged $A_{\text{cell}}=1590\pm 54 \mu\text{m}^2$ was selected for motifs design (Data is shown as mean \pm SEM). Inset, a cell completely spread of a single fibronectin asymmetric motif (scale bar = $50 \mu\text{m}$). (c) Functionalization protocol (see Methods). (i) Glass coverslips #1 were thoroughly cleaned and chemically activated with 'Piranha' solution. (ii) Glass coverslips were silanized by vapor phase methodology with 3-(mercaptopropyl)trimethoxysilane and placed in the oven at 65°C for 4 hours. (iii) Microcontact printing technique was used to deposit the fibronectin pattern on the substrate. (iv) Non-functionalized regions were blocked with poly(L-lysine)-g-poly(ethylene glycol) (PLL-g-PEG). The sample was stored in PBS (pH 7.4) at 4°C at least 30 minutes prior to use.



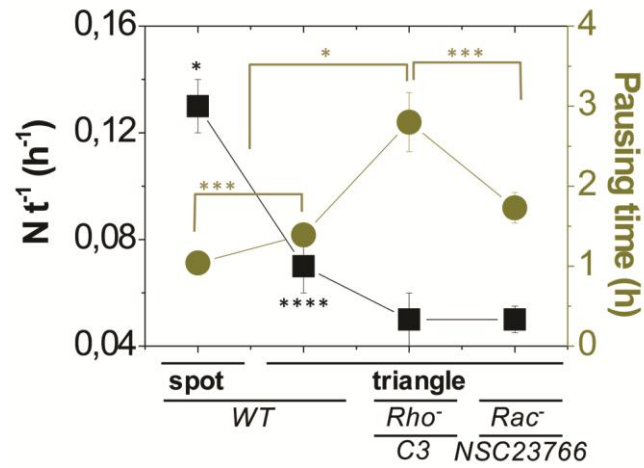
Supplemental Figure SF3. Length of protrusions extension. Average protruding distance d_p in the + and - directions. Cells extend protrusions of similar length in all directions for each condition. (Data set: WT=885; C3-Rho= 1084 and NSC23766-Rac⁻= 1084 analyzed filopodia. N=3). Data are presented as mean \pm SD. * $P < 0.05$ (Student's t-test).



Supplemental Figure SF4. Internal polarity caused by the asymmetric fibronectin ratchet. (a). NIH3T3 cells were deposited on $10 \mu\text{g ml}^{-1}$ rhodamine-labelled fibronectin spots by microcontact printing on a glass coverslip (see Methods). Cells were allowed to spread prior fixation. Afterwards, cells were stained for nucleus (blue) and centrosome (green). The position of the centrosome was measured with respect to the nucleus (see Methods). Scale bar: $15 \mu\text{m}$. **(b).** Circular histogram of the spatial distributions for the centrosome with respect to the nucleus centroid ($n=199$ cells) of cells plated on fibronectin spots showing an isotropic distribution. **(c).** Fixation and staining for the nucleus (blue) and centrosome (green) of NIH3T3 cells on rhodamine-labelled fibronectin ($10 \mu\text{g ml}^{-1}$) asymmetric triangles. The position of the centrosome was again measured with respect of the nucleus. Scale bar: $15 \mu\text{m}$. **(d).** Circular histogram of the spatial distributions of the centrosome with respect to the nucleus centroid. ($n=101$ cells). The histogram shows a distribution of the centrosomes along the longest axis and a bias towards the wide edge.



Supplemental Figure SF5. Rho and Rac pathway inhibitions cause a clear effect on cell cytoskeleton structure. Cells were deposited on a microcontact printed glass coverslip with a $10 \mu\text{g ml}^{-1}$ fibronectin concentration. We compared the effect of Rho and Rac pathways inhibition on cell cytoskeleton when treated with the inhibitors C3 transferase (80 nM) and NSC23766 (100 μM). Cells were labeled for actin and paxillin. Right column shows the incubation time at fixation; note that the same phenotype was observed throughout the experiment. Scale bar = 20 μm .



Supplemental Figure SF6. Long-term cell motion characterization. (*Left*) Number of changes of direction per unit of time for all the conditions. Cells switch direction more often for *WT*-spot condition. Data suggest a more directional motion in the ratchet configuration for *Rho⁻* and *Rac⁻*. (*Right*) Pausing time (T_{pa}) prior a direction change for all the conditions. For *Rho⁻* cells show the highest T_{pa} value.

3. Supplemental Model Description

3.1 Probabilistic model for the direction index I_{dir}

We here show a simple model that predicts the probability p_+ that a protrusion is stabilized in the + rather than - direction for a cell on a 1d lattice of triangular adhesive patterns, and show that the direction index I_{dir} quantifies the asymmetry of this quantity $I_{dir} = p_+ - p_-$. The width and height of a triangular region is h and w , respectively (we here follow the notation in Supplementary Figure 2). The length of the gap between two nearest adhesive regions is a_1 . In many cases, cells plated on these adhesive triangular regions spread in the shape of these regions. These cells extend protrusions to the nearest adhesive regions at the right and left. We here treat the case that the probability distribution that an extended protrusion has the length l has the form

$$\psi(l) = \lambda e^{-\lambda l} \quad (1)$$

, where λ^{-1} is the average length of protrusions. This exponential form of the probability distribution was shown experimentally by Xia *et al* [23]. Cells extend n_+ (multiple) protrusions towards the right and n_- protrusions towards the left at the same time (where $n_+ \neq n_-$ for the case of cells on triangular patterns because of cell polarization) with frequency $1/\tau_p$. The probability ψ_+ that a protrusion extended towards the right touches the adhesive region at the nearest neighbor is derived by integrating $\psi(l)$ in the adhesive regions at the nearest neighbor and has the form

$$\psi_+ = g_+ e^{-\lambda a_1}, \quad (2)$$

where g_+ is the geometrical factors (that include the information of the geometry of adhesive regions) for protrusions towards the right and has the form

$$g_+ = 1 - \frac{1}{\lambda h} (1 - e^{-\lambda h}). \quad (3)$$

In a similar manner, the probability that a protrusion extended towards the left touches the adhesive region at the nearest neighbor has the form

$$\psi_- = g_- e^{-\lambda a_1}, \quad (4)$$

where g_- is the geometrical factors for protrusions towards the left and has the form

$$g_- = \frac{1}{\lambda h} (1 - e^{-\lambda h}) - e^{-\lambda h}. \quad (5)$$

The inequality $g_+ \neq g_-$ reflects the fact that the accessible adhesive area is different for protrusions extended towards the right and left.

Because of the relatively large gap between adhesive regions, cells must exert forces that are larger than a threshold value to move from one adhesive regions to the others. This requires a coordinated dynamics between protrusions and retraction, and therefore requires that protrusions are stabilized. We here assume that this stabilization occurs with the Poisson process of rate β . Our experiments show that the stabilization time, during which a protrusion is stabilized on adhesive regions, depends on whether this protrusion is extended towards the right or left, probably due to cell polarization. A protrusion that touches the (nearest) adhesive regions at the right is stabilized with probability

$$s_+ = 1 - e^{-\beta \tau_+}, \quad (6)$$

where τ_+ is the stabilization time for protrusions extended towards the right. The probability s_- a protrusion that touches the adhesive region at the left is stabilized has a similar form, but with the stabilization time is τ_- . With this model, the total number of protrusions that are extended towards the right is $n_+ \tau_0 / \tau_p$, where τ_0 is the duration time that a cell stays in the same adhesive region before moving to the next region. Among these protrusions, the ratio of protrusions that touch the nearest adhesive region is ψ_+ , and those protrusions that touch to the adhesive region are stabilized and become efficient with the probability s_+ . The probability that a protrusion is stabilized at the right rather than the left thus

has the form

$$p_+ = C v_+ \tau_0 s_+, \quad (7)$$

where $v_+ = n_+ \psi_+ / \tau_p$ is the frequency of protrusions that touch the nearest adhesive region. In a similar manner, the probability that a protrusion is stabilized at the left rather than the right is derived in the form

$$p_- = C v_- \tau_0 s_-, \quad (8)$$

where the normalization constant C is deduced from

$$C^{-1} = v_+ s_+ \tau_0 + v_- s_- \tau_0, \quad (9)$$

which implies that the protrusion is stabilized either on the + or – side. One then obtains:

$$\begin{aligned} p_+ - p_- &= \frac{v_+ s_+ - v_- s_-}{v_+ s_+ + v_- s_-} \\ &\approx \frac{v_+ \tau_+ - v_- \tau_-}{v_+ \tau_+ + v_- \tau_-} = I_{dir} \end{aligned} \quad (11)$$

The last equation of the right hand side was derived by assuming that the rate β is much smaller than the inverse of stabilization time (for both protrusions towards the right and left). This equation is indeed equal to the direction index I_{dir} defined in eq. (1) of the main text with $z_+ = v_+ s_+$ and $z_- = v_- s_-$, and provides a probabilistic interpretation of the direction index.

3.2 Persistent random walk model – long time motion

The model aims at linking the observed persistence and asymmetry in the +/- directions of the trajectories to the fluctuation dynamics of the protrusions. The persistent random walk model is defined as follows. A cell trajectory is discretized, each elementary step being defined as a transition from one adhesive motif to a neighboring motif, either in the + or – direction. One then introduces the

conditional transition probabilities π_{ji} where $i, j = +, -$, which are defined as the probability that a cell performs a step in the direction j , knowing that the previous step was performed in direction i . Normalization then imposes $\pi_{+i} + \pi_{-i} = 1$, so that only two quantities (π_{++} and π_{--} for example) are independent. The π_{ji} encode two effects responsible for the direction of migration: the asymmetry of the adhesive motifs and the direction of the previous move. The observation that $\pi_{i+} \neq \pi_{i-}$ (see Figure 4 of the main text) clearly shows that the memory of the previous move, which is likely to affect the internal organization of organelles, influences the direction of the upcoming move. We now show that the main characteristics of the trajectories can be expressed in terms of the π_{ji} . The analysis of the stationary state shows that the probability Π_+ of observing a step in the + direction (with no knowledge of the previous step) reads

$$\Pi_+ = \frac{1 - \pi_{--}}{2 - (\pi_{++} + \pi_{--})} \quad (12)$$

The corresponding quantity Π_- is then obtained by substituting $+\leftrightarrow-$. The bias (measured experimentally as the R/L ratio) is then conveniently quantified by

$$\frac{\Pi_+}{\Pi_-} = \frac{1 - \pi_{--}}{1 - \pi_{++}} \quad (13)$$

The persistence length in the +/- direction is readily obtained in the case of infinitely long trajectories as

$$L_p^\pm = \frac{1}{1 - \pi_{\pm\pm}} \quad (14)$$

In experiments, the trajectories are finite, either because of the finite observation time, or because of cells making pauses. These effects are accounted for, by defining the probability q that a trajectory ends at each step. One then obtains the following expression of the persistence length, which is used to analyze the experimental data:

$$L_p^\pm = \frac{1}{1 - (1-q)\pi_{\pm\pm}} \quad (15)$$

Figure 4 of the main text shows that using the measured values of the π_{ji} , the predictions of both the R/L ratio (quantified by Π_+/Π_-) and the persistence lengths are in very good agreement with observations in all tested conditions. This proves that the cell trajectories are well described by the persistent random walk model.

3.3 Probabilistic model for transition probabilities π_{ji}

We next aimed at linking the π_{ji} to the protrusion activity by extending the model described in 2.1, and made use of the parameters accessible experimentally: the number of protrusions (per unit time) hitting the adhesive region in the direction + (resp. -) denoted by ν_+ (resp. ν_-), and the corresponding probability that a protrusion is stabilized and eventually mediates a force denoted by s_+ (resp. s_-). These quantities then enable the definition of the mean number (per unit time) of stabilized protrusions $z_i = s_i \nu_i$, where $i=+,-$. Following the argument in 2.1, z_i has an asymptotic form $z_i \approx \beta \tau_i \nu_i$ where τ_i is the average time that a protrusion is stabilized on the adhesive motif. Following the finding that the direction of motion depends on the direction of the previous move, the quantities s_i, ν_i, τ_i, z_i in fact depend also on the direction of the previous move and should be written as $s_{ji}, \nu_{ji}, \tau_{ji}, z_{ji}$. One can then define the probability $p(n_+)$ that n_+ protrusion are stabilized at the + edge (and similarly at the - edge), which are classical binomial distribution. We will make use of the following Poisson approximation

$$p(n_+) = \frac{(z_+ \tau_0)^{n_+}}{n_+!} e^{-z_+ \tau_0} \quad (16)$$

where τ_0 is the duration time that a cell stays on one motif and the dependence on the previous move is omitted for clarity. We then introduce the asymmetry of stabilized protrusions $\Delta = n_+ - n_-$. This

quantity is distributed according to

$$P(\Delta) = e^{-(z_+ + z_-)\tau_0} \left(\frac{z_+}{z_-} \right)^{\Delta/2} I_{\Delta} \left(2\tau_0 \sqrt{z_+ z_-} \right) \quad (17)$$

where $I_D(x)$ is the first kind modified Bessel function of D -th rank. Note that the average of Δ is, up to a normalization constant, the direction index I_{dir} derived in eq. (11). We then hypothesized that the direction of motion at each step is dictated by the edge having the largest number of stabilized protrusions. This condition $\Delta \geq 1$ enables an explicit calculation of π_{ji} that reads:

$$\pi_{ji} = e^{-(z_{ji} + z_{-ji})\tau_0} \sum_{\Delta \geq 1} \left(\frac{z_{ji}}{z_{-ji}} \right)^{\Delta/2} I_{\Delta} \left(2\tau_0 \sqrt{z_{ji} z_{-ji}} \right). \quad (18)$$

Clearly, this quantity can be expressed in terms of I_{dir} and an auxiliary variable (for example $(z_{ji} + z_{-ji})\tau_0$). This shows that the knowledge of the protrusion activity, encoded in z_{ji} and therefore I_{dir} enables the determination of the transition probabilities π_{ji} that determine the large scale properties of the trajectories.

4. Supplemental Movie Titles and Legends.

Supplemental Movie SM1 – Protrusions probing activity on a FN ratchet. Movie of an individual NIH3T3 fibroblast showing the different steps of cell protruding activity prior to cell migration. Cell starts to fluctuate after cell spreading and polarization on the adhesive fibronectin ratchet generating a cell front and a cell rear. Colored arrows (blue and green) highlight the effective probing of the protrusions on the neighboring adhesive motifs. Yellow arrows determine the start of cell spreading, migration and the retraction at the back of the cell. Acquisition time: 1 image / 30 seconds. Time in hh:mm:ss. (Scale bar: 50 μm).

Supplemental Movie SM2 – Protrusions probing activity on a triangle with 2 symmetric rectangles. Protrusions activity study of a cell spread on a FN triangle with rectangle-shaped neighboring motifs on both sides. Colored arrows (blue and green) highlight the effective probing of the protrusions on the neighboring adhesive motifs. Yellow arrows determine the start of cell spreading and migration. Acquisition time: 1 image / 30 seconds. Time in hh:mm:ss. (Scale bar: 50 μm).

Supplemental Movie SM3 – Protrusions probing activity on a spot with 2 symmetric neighboring rectangles. Protrusions activity study of a cell spread on a FN spot with rectangle-shaped neighboring motifs on both sides. Colored arrows (blue and green) highlight the effective probing of the protrusions on the neighboring adhesive motifs. Yellow arrows determine the start of cell spreading and migration. Acquisition time: 1 image / 30 seconds. Time in hh:mm:ss. (Scale bar: 50 μm).

Supplemental Movie SM4 – Fluctuating cell on a fibronectin spot pattern. Movie of an individual NIH3T3 fibroblast for 48 hours fluctuating from one fibronectin spot (in red) to the neighboring ones crossing the PLL-g-PEG blocked regions and changing its direction of migration. Acquisition time: 1 image / 5 minutes. Time in hh:mm. (Scale bar: 100 μm).

Supplemental Movie SM5 – Cell motion on a sequence of fibronectin triangular patches. Movie of an individual NIH3T3 fibroblast for 30 hours plated on a sequence of micropatterned fibronectin triangular patches (in red). The cell fluctuates right and left at the beginning of the movie from one fibronectin triangle to the neighboring ones crossing the PLL-g-PEG blocked regions. Then, the cell migrates directionally in the direction of sharp edge of the triangle (+ end). Acquisition time: 1 image / 5 minutes. Time in hh:mm. (Scale bar: 100 μm).